ISSN 1029-9599, Physical Mesomechanics, 2018, Vol. 21, No. 4, pp. 314–319. © Pleiades Publishing, Ltd., 2018.
Original Russian Text © T.V. Tretyakova, V.E. Wildemann, 2017, published in Fizicheskaya Mezomekhanika, 2017, Vol. 20, No. 2, pp. 71–78.

Plastic Strain Localization and Its Stages in Al–Mg Alloys

T. V. Tretyakova[1]* and V. E. Wildemann[1]

[1] *Perm National Research Polytechnic University, Perm, 614990 Russia*
** e-mail: cem.tretyakova@gmail.com*

Received April 10, 2017

Abstract—The paper describes an experimental technique based on the use of a Vic-3D contactless digital optical system and digital image correlation for research in the mechanical behavior of a solid and its plastic deformation with space-time inhomogeneities. Using this technique, we analyze the evolution of inhomogeneous strain and local strain rate fields in AMg2m alloy at constant uniaxial tension rates. The analysis reveals quasi-periodic strain field homogenization in jerky flow: alternating phases of active local plastic flow (shear banding) and macroscale strain levelling. Also analyzed are the parameters of localized microscale plastic flow such as the height and width of shear bands, their velocity, and coefficient of plastic strain inhomogeneity. From a series of mechanical tests, the influence of the specimen geometry and loading rate on these parameters is estimated.

DOI: 10.1134/S1029959918040057

Keywords: digital image correlation, Al–Mg alloy, yield delay, Chernov–Lüders band, jerky flow, Portevin–Le Chatelier effect, plastic strain localization

1. INTRODUCTION

Now, complex research methods are needed to deeply understand the mechanisms of plastic deformation in structural metals and alloys [1–7]. The accuracy of research data and their value can be greatly increased if testing equipment is used jointly with high-precision measuring instruments, contactless recording systems, and nondestructive techniques [8–11]. One of the efficient optical methods is digital image correlation [8, 9, 11–14], which allows one to analyze and quantitatively estimate the inhomogeneity of inelastic strains in materials with clearly defined macroscale strain localization on their surface.

Research data suggest that only a series of alloys feature strain inhomogeneity in space and time. For example, the stress–strain diagram of low-carbon steels reveals a sharp yield point, a yield plateau, and Chernov–Lüders bands propagating on their surface [3–5, 8, 15, 16]. In a loaded Al–Mg alloy, serrated yielding with numerous peaks and dips is observed being indicative of the Portevin–Le Chatelier effect [1, 3, 4]. At the softening stage of tensile materials, such strain inhomogeneity results in necking, and due to defect accumulation, their stress–strain curves reveal a descending portion of supercritical or so-called postcritical strains [17–19].

Here, using experimental data and digital image correlation, we study the mechanical behavior of an Al–Mg alloy featuring spatial-temporal strain inhomogeneities, analyze the parameters of macroscale strain localization in the material, and assess the influence of its geometry and loading rate on its deformation.

2. MATERIAL AND RESEARCH TECHNIQUE

The test material was as-received AMg2m rolled sheets (2.2Mg, 0.6Mn, 0.4Fe, 0.4Si, %). The material was machined by hydro-abrasive cutting to obtain two groups of flat dumbbell-shaped specimens differing in thickness h, gage section length l_0 and width b_0, and shoulder radius r_0: (i) h = 2 mm, l_0 = 50 mm, b_0 = 12 mm, r_0 = 5 mm; (ii) h = 3 mm, l_0 = 75 and 100 mm, b_0 = 10 mm, r_0 = 5 mm. The specimens were exposed to uniaxial tension at room temperature (22–23°C) on an Instron 8850 biaxial (tension/torsion) servohydraulic machine with crosshead velocities $\dot{u}_0$ = 0.5–10 mm/min, which correspond to strain rates $\dot{\varepsilon}_0$ from 1.67×10^{-4} to 33.33×10^{-4} s^{-1}.

The mechanisms of inelastic deformation were studied using a Vic-3D contactless digital optical system (Correlated Solutions) designed for recording displacement and strain fields on the surface of test specimens and structural elements of various geometries, states in stress concentrator zones, defect accumulation, and fracture. Its mathematical software is based on digital image correlation [14].

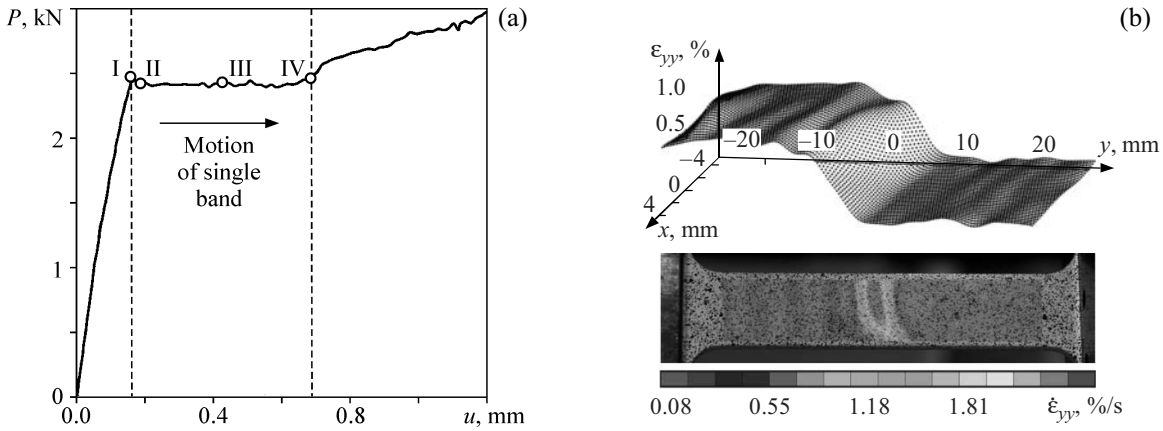

Fig. 1. Propagation of a single Chernov–Lüders band during the formation of yield plateau: initial portion $P \sim u$ (a) and fields ε_{yy} and $\dot{\varepsilon}_{yy}$ at $t = t_{III}$ (b).

In the study, we used black-and-white digital cameras with a resolution of 4.0 and 16.0 Mpx, special imaging control software (Vic-Snap) and image processing software (Vic-3D), an illumination system, a synchronizer of the video system and controller of the testing machine, and a set of calibration tables [20]. The imaging speed was 10–50 frm/s. The images were processed using the so-called NSSD criterion (normalized sum of squared differences). The fields of longitudinal ε_{yy}, transverse ε_{xx}, and shear strains ε_{xy} were calculated using the Lagrangian finite strain tensor with the *Oy* axis directed along the tension axis and *Ox* axis perpendicular to it.

3. PLASTIC STRAIN INHOMOGENEITY IN TENSILE Al–Mg ALLOY

The distributions of displacement fields, and strain and local strain rate fields in the test specimens of the first group ($b_0 = 12$ mm, $l_0 = 50$ mm) suggest the following. At the elastic stage till the upper yield point is reached ($\sigma \le \sigma_y^u$), the strain field distribution is macrohomogeneous. The mean of longitudinal strains over the specimens is $\varepsilon_m = 18\%$ at $t = t_I$.

The transition from the upper to the lower yield point ($\sigma = \sigma_y^b$) corresponds to the instant at which a Chernov–Lüders band arises as evidence of active plastic strain localization. On the specimen surface near the grips, the longitudinal strain increases steeply to $\varepsilon_{yy} = 0.93\%$. The local strain rate at the band front reaches $\dot{\varepsilon}_{yy} = 2.66\%/s$. It should be noted that the propagation region of the Chernov–Lüders front in the material suspends its deformation up to the onset of hardening. The macroscale strain in the material is incremented due to its elongation in the region preceding the band at the stage of yield delay [15]. Figure 1 shows the configuration of inhomogeneous longitudinal strain fields ε_{yy} and local longitudinal strain rates $\dot{\varepsilon}_{yy}$ for the specimens with $b_0 = 12$ mm and $l_0 = 50$ mm deformed at $\dot{\varepsilon}_0 = 1.67 \times 10^{-4}$ s^{-1} [21].

Table presents data demonstrating the dependence of the Chernov–Lüders band velocity on the loading rate $\dot{\varepsilon}_0$ in the range from 1.67×10^{-4} to 33.33×10^{-4} s^{-1} for the specimens with $h_0 = 2$ mm and $b_0 = 12$ and 20 mm.

The parameters in the table include the coefficient of plastic strain inhomogeneity k_b, which is the ratio of the grip velocity $\dot{u}_0$ to the shear band velocity v_b, and mean longitudinal strain ε_a attained after passage of the Chernov–Lüders band. For the specimens with a gage section of width $b_0 = 12$ mm, the average strain inhomogeneity coefficient is $k_b = 0.01$, and for those with $b_0 = 20$ mm, it is $k_b = 0.011$. The maximum difference is 23.4%, i.e., the values are of the same order. The mean strain at the band front is $\varepsilon_a = 1.26\%$ (table).

Relationship between shear band velocities and loading rates

$\dot{u}_0$, mm/min	v_b, mm/min	k_b	ε_b, %	$\dot{u}_0$, mm/min	v_b, mm/min	k_b	ε_b, %
$b_0 = 12$ mm				$b_0 = 20$ mm			
0.5	55.2	0.009	1.29	1.0	98.4	0.010	1.21
1.0	104.6	0.010	1.20	1.0	92.0	0.011	1.22
1.0	97.6	0.010	1.17	5.0	422.9	0.012	1.35
5.0	458.5	0.011	1.28	10.0	845.1	0.012	1.36

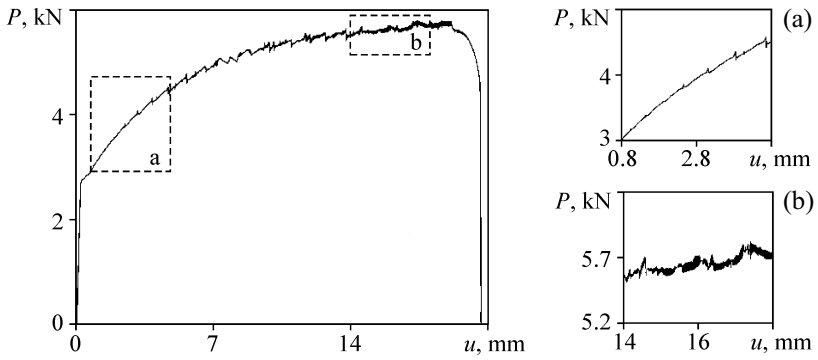

Fig. 2. Loading diagram of AMg2m ($b_0 = 10$ mm, $l_0 = 100$ mm, $h_0 = 3$ mm).

At the hardening stage, the material reveals serrated deformation (Portevin–Le Chatelier effect) with numerous peaks and dips [1, 4]. Figure 2 shows a typical loading diagram with a serrated portion for the Al–Mg specimens with a gage section of length $l_0 = 100$ mm, width $b_0 = 10$ mm, and thickness $h_0 = 3$ mm. As can be seen, strain localization bands appear on the specimen surface.

Figure 3 shows the fields of local strain rates along the axes $Oy\,(\dot{u}_y)$, $Ox\,(\dot{u}_x)$, and $Oz\,(\dot{u}_z)$, with Oz being perpendicular the specimens plane. Research data on the evolution of strain inhomogeneity in flat Al–Mg specimens during the formation and motion of single Portevin–Le Chatelier bands, which show up as serrations on loading diagrams, can be found elsewhere [21]. It should be noted that the angle between the Portevin–Le Chatelier band and the loading axis is ±59°.

4. QUASIPERIODIC PLASTIC STRAIN HOMOGENIZATION IN SERRATED YIELDING

In analyzing the patterns of strain fields, one can distinguish a certain periodicity of macroscale plastic strain localization in the presence of Portevin–Le Chatelier bands [22]. Figure 4 shows a series of $\varepsilon_{yy} \sim y$ profiles with the origin of coordinates in the gage section center at equal time intervals Δt for the specimens with $b_0 =$ 10 mm, $l_0 = 100$ mm, and $h_0 = 3$ mm deformed by uniaxial tension at a rate $\dot{\varepsilon}_0 = 1.67 \times 10^{-3}$ s^{-1} ($\Delta t = 2$ s). The profiles correspond to the formation and propagation of a single Chernov–Lüders band at the stage of yield delay. The level of longitudinal strain ε_a attained after passage of the band front is marked by a dashed line, and the motion direction of the band is indicated by an arrow v_b. As the band front reaches the opposite grip, the longitudinal strain becomes macrohomogeneous (Figs. 4 and 5, curve *0*) and relatively leveled.

It is of interest to analyze the inhomogeneity resulting from several strain localization bands. Figure 5 shows a series of longitudinal strain profiles at the stages of elastoplastic deformation and hardening. The stage of supercritical deformation is not considered, because of the high degree of plastic strain localization in the neck region. The time interval is $\Delta t = 2$ s; the origin of coordinates is at the center of the specimen gage section. The specimen surface reveals alternating phases of active lo-

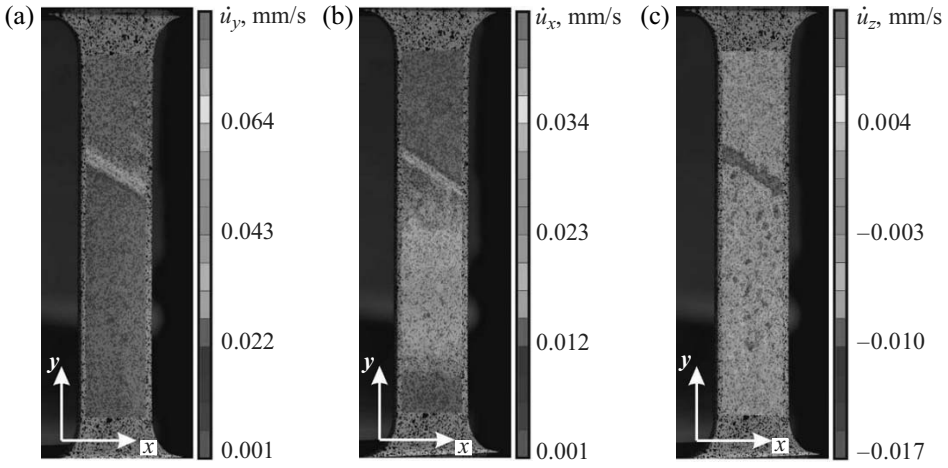

Fig. 3. Inhomogeneous fields $\dot{u}_y$ (a), $\dot{u}_x$ (b), and $\dot{u}_z$ (a) for a Portevin–Le Chatelier band on the flat surface of AMg2m alloy.

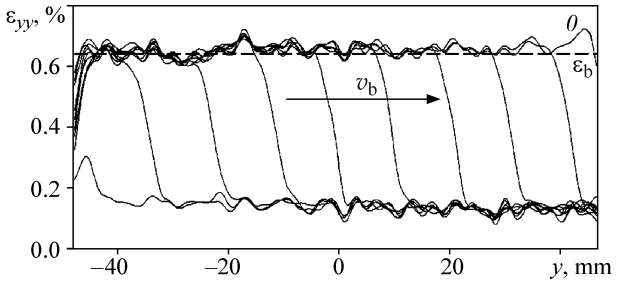

Fig. 4. Longitudinal strain profiles ε_{yy} in AMg2m during the formation of a yield plateau.

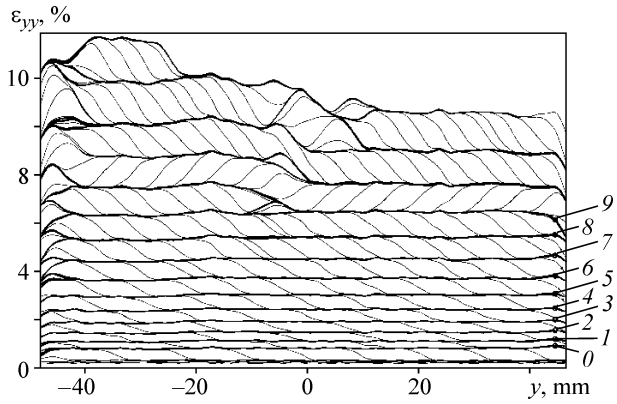

Fig. 5. Strain profiles ε_{yy} in AMg2m at the stages of elastoplastic deformation and hardening.

cal plastic flow (shear banding) and macroscale strain leveling over the material. In Fig. 5, the propagation of single strain localization bands is illustrated by slant lines; curves *0–9* correspond to the instant of relative homogenization of longitudinal strains over the surface. Noteworthy are quasiperiodic patterns of inhomogeneous inelastic strain fields at the stage of jerky plastic flow in AMg2m alloy [22].

This regularity can be illustrated by the time dependence of the mean longitudinal strain $\Delta\varepsilon_{yy}$ (Fig. 6) at the points of strain levelling *0–9* (Fig. 5). The quantity $\Delta\varepsilon_{yy}$ is the difference between the average levels of longitudinal strains ε_{yy} for the nth and $(n-1)$th profile (Fig. 5). This linear dependence can be approximated by $\Delta\varepsilon_{yy} = 0.022t + 0.28\%$.

The degree of macroscale strain localization can be estimated from the time dependence of the coefficient of plastic strain inhomogeneity: $k_{\text{PLC}} = \varepsilon_{yy}^{\max} / \varepsilon_{yy}^{\text{mean}}$, where $\varepsilon_{yy}^{\max}$ is the maximum longitudinal strain and $\varepsilon_{yy}^{\text{mean}}$ is the mean strain for each frame (Fig. 7). When the strain field distribution over the specimen surface is macrohomogeneous, this coefficient is close to unity. When a zone of active plastic flow arises, the curve $k_{\text{PLC}} - t$ reveals a sharp peak because the strain at the band front is much higher. As the band propagates along the specimen and the longitudinal strain levels off, the inhomogeneity coefficient decreases gradually. As the macroscale strain increases, the amplitude of jumps increases and so does the time intervals between them.

5. STAGES OF PLASTIC STRAIN LOCALIZATION IN INELASTICALLY DEFORMED Al–Mg ALLOY

Reasoning from the evolution of strain inhomogeneity in the Al–Mg specimens under uniaxial tension, we can consider a certain stage model of inelastic deformation and macroscale plastic strain localization associated with Chernov–Lüders bands and Portevin–Le Chatelier effect.

Stage I represents macrohomogeneous deformation till the upper yield point is reached $(\sigma \le \sigma_y^u)$. The main parameter of stage I is the strain accumulated to the point at which a strain localization band arises (ε_ξ). The results of tests at the specified strain rates suggest that this strain does not depend on the rate of external loading and its mean is $\varepsilon_\xi = 0.13\%$.

Stage II represents the formation and propagation of a Chernov–Lüders band with yield delay. The transition

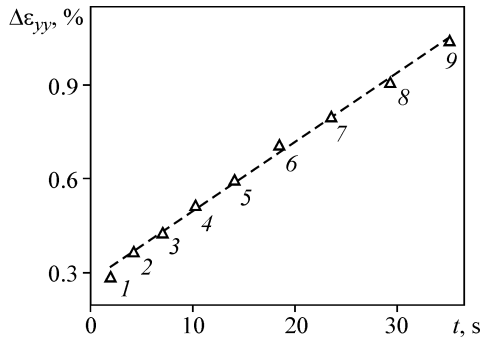

Fig. 6. Dependence $\Delta\varepsilon_{yy} \sim t$ for periodic macrostrain leveling.

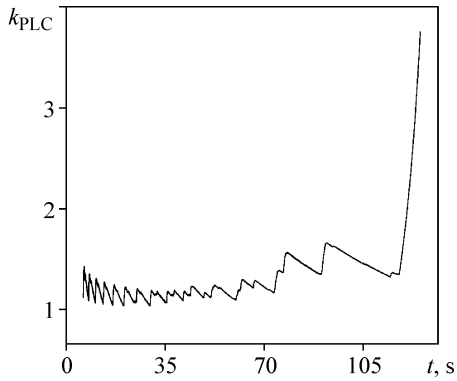

Fig. 7. Coefficient of plastic strain inhomogeneity k_{PLC} as a function of time.

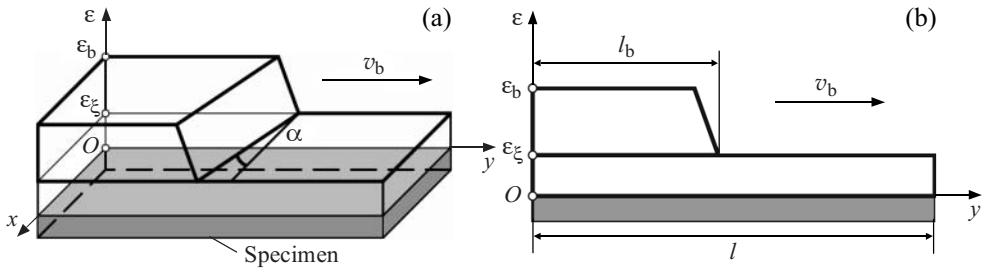

Fig. 8. Longitudinal strain distribution over the specimen surface during the formation of a yield plateau.

from the upper σ_y^u to the lower yield point σ_y^b corresponds to the instant at which the material is involved in active plastic flow. Under further loading, the region of plastic deformation develops, and the band front separating the elastic part from plastic moves along the specimen toward the opposite grip. Figure 8 shows a schematic representation of the longitudinal strain field during the formation of a yield plateau.

The propagation of a Chernov–Lüders band can be characterized by the following parameters: the strain ε_a accumulated after passage of the band front or the front height, the band velocity v_b, and the angle α between the band front and the axis Ox (Fig. 8). Also indicated in Fig. 8 are the distance l_b travelled by the band and the total specimen length l. As can be seen from table, the average height of the band front is $\varepsilon_a = 1.26\%$. At the point of transition to hardening, no matter where the Chernov–Lüders band arises, one more relative leveling of macroscale strains occurs

The introduced parameters allow us to refine the meaning of the coefficient of plastic strain inhomogeneity k_b. Because

$$u_0 = \varepsilon_a l_b + \varepsilon_\xi (l - l_b), \tag{2}$$

it is obvious that

$$\dot{u}_0 = \varepsilon_a v_b - \varepsilon_\xi v_b = (\varepsilon_a - \varepsilon_\xi) v_b. \tag{3}$$

Hence,

$$k_b = \varepsilon_a - \varepsilon_\xi. \tag{4}$$

Stage III represents the formation and motion of Portevin–Le Chatelier bands associated with serrated yielding in Al–Mg at its hardening stage. Figure 9 shows a schematic representation of the initiation and evolution of active plastic flow during the propagation of a single band.

Stage III with its jerky plastic flow features quasiperiodic patterns of inhomogeneous strain fields with alternating phases of active plastic flow (shear banding) and macroscale strain levelling (Fig. 10). After passage of a single Portevin–Le Chatelier band, the longitudinal strain takes on the value $\varepsilon_{yy} = \varepsilon_{PLC}^{(1)}$ at $t = t_1$, and at $t = t_2$ and $t = t_n$, it reaches $\varepsilon_{yy} = \varepsilon_{PLC}^{(2)}$ and $\varepsilon_{yy} = \varepsilon_{PLC}^{(n)}$, respectively.

Stage IV represents the formation of a neck in the lateral section of the material as the final stage of its deformation (softening).

6. CONCLUSION

Thus, we have analyzed the space-time inhomogeneity of plastic flow in AMg2m alloy with yield delay and serrated yielding under uniaxial tension at constant rates. Our analysis of loading diagrams, fields of longitudinal, transverse, and shear strains and local strain rates, and their time dependences shows that the inhomogeneity of strain fields at the stage of serrated deformation evolves quasiperiodically through alternating phases of active plastic flow (shear banding) and macroscale strain levelling. The analysis also provides estimates of the effect of the specimen geometry and loading rate on a series of parameters descriptive of the strain inhomogeneity induced by Chernov–Lüders and Portevin–Le Chatelier bands.

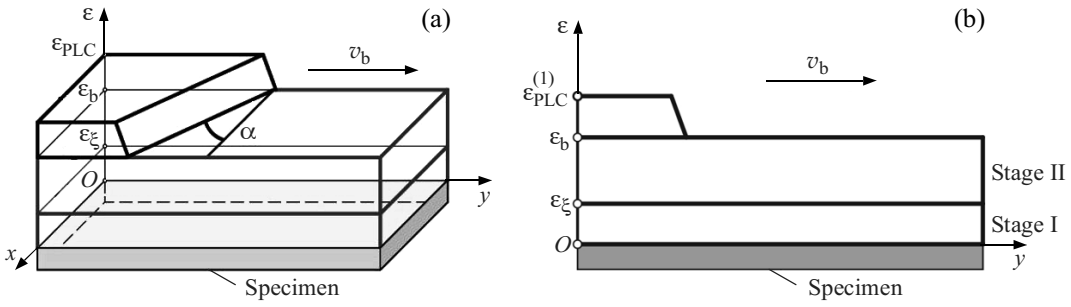

Fig. 9. Schematic representation of the formation and motion of a single strain band in jerky flow (Portevin–Le Chatelier effect).

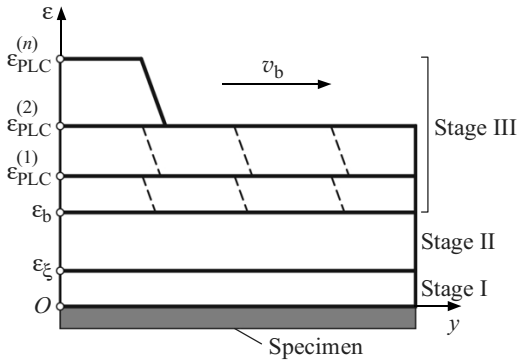

Fig. 10. Quasiperiodic patterns of inhomogeneous inelastic strain fields.

ACKNOWLEDGMENTS

The work was performed at Perm National Research Polytechnic University, Center of Experimental Mechanics, and was supported by RSF project No. 16-19-00069.

REFERENCES

1. Deryugin, Ye.Ye., Panin, V.E., Schmauder, S., and Suvorov, B.I., Study of Local Characteristics of Jerky Flow for Particle Reinforced Aluminum as a Multilevel System, *Fiz. Mezomekh*., 2006, vol. 9, no. 5, pp. 27–32.
2. Egorushkin, V.E., Panin, V.E., and Panin, A.V., Influence of Multiscale Localized Plastic Flow on Stress-Strain Patterns, *Phys. Mesomech.*, 2015, vol. 18, no. 1, pp. 8–12.
3. Zuev, L.B., Danilov, V.I., and Barannikova, S.A., *Physics of Plastic Flow Macrolocalization*, Novosibirsk: Nauka, 2008.
4. Krishtal, M.M., Instability and Mesoscopic Inhomogeneity of Plastic Deformation (Analytical Review). Part I. Phenomenology of Yield Drop and Jerky Flow, *Phys. Mesomech*., 2004, vol. 7, no. 5–6, pp. 5–26.
5. Krishtal, M.M., Instability and Mesoscopic Inhomogeneity of Plastic Deformation (Analytical Review). Part II. Theoretical Views on Mechanisms of Plastic Deformation Instability, *Phys. Mesomech*., 2004, vol. 7, no. 5–6, pp. 27–40.
6. Panin, V.E., Egorushkin, V.E., Panin, A.V., and Chernyavskii, A.G., Plastic Distortion as a Fundamental Mechanism in Nonlinear Mesomechanics of Plastic Deformation and Fracture, *Phys. Mesomech*., 2016, vol. 19, no. 3, pp. 255–268.
7. Sokovikov, M.A., Bayandin, Yu.V., Lyapunova, E.A., Plekhov, O.A., Chudinov, V.V., and Naimark, O.B., Plastic Shear Localization and Fracture Mechanisms in Metals under Dynamic Loading, *Vychisl. Mekh. Splosh. Sred*, 2013, vol. 6, no. 4, pp. 467–474.
8. Avril, S., Pierron, F., Sutton, M.A., and Yan, J., Identification of Elasto-Plastic Parameters and Characterization of Luders Behavior Using Digital Image Correlation and the Virtual Fields Method, *Mech. Mater.*, 2008, vol. 40, pp. 729–742.
9. Bashkov, O.V., Panin, S.V., and Byakov, A.V., Acoustic Emission, Digital Image Correlation and Loading Diagram Analysis of the Effect of the Nitrided Surface Layer Thickness on the Stage Character of Deformation and Fracture of 12Cr18Ni10Ti Steel, *Fiz. Mezomekh*., 2010, vol. 13, no. 6, pp. 53–72.
10. Larichkin, A.Yu., Kornev, V.M., and Demeshkin, A.G., Plasticity Zone Change and Damage Accumulation with Crack Growth under Low-Cycle Loading of Quasi-Brittle Materials, *Fiz. Mezomekh*., 2016, vol. 19, no. 4, pp. 38–48.
11. Panin, S.V., Bashkov, O.V., Semashko, N.A., Panin, V.E., and Zolotareva, S.V., Combined Study of Deformation Peculiarities of Flat and Notched Specimens at the Micro- and Mesolevels by Means of Acoustic Emission Method and Surface Strain Mapping, *Fiz. Mezomekh*., 2004, vol. 7, spec. iss., part 2, pp. 303–306.
12. Panin, S.V., Titkov, V.V., and Lyubutin, P.S., Efficiency of Vector Field Filtration Algorithms in Estimating Material Strain by the Method of Digital Image Correlation, *Optoelectron. Instrum. Data Process.*, 2013, vol. 49, no. 2, pp. 155–163.
13. Panin, S.V., Titkov, V.V., and Lyubutin, P.S., Smoothing of Vector Fields by Using the Bezier Surface for Strain Estimation by the Method of Digital Image Correlation, *Optoelectron. Instrum. Data Process.*, 2014, vol. 50, no. 1, pp. 61–67.
14. Sutton, M.A., Orteu, J.-J., and Schreier, H., *Image Correlation for Shape, Motion and Deformation Measurements*, Columbia, SC, USA: University of South Carolina, 2009.
15. Lomakin, E.V. and Melshanov, A.F., Behavior of Low-Carbon Steel in Tension, *Izv. Akad. Nauk SSSR*, *Mekh. Tverd. Tela*, 1971, no. 4, pp. 150–158.
16. Rabotnov, Yu.N. and Suvorova, Yu.V., Law of Deformation of Metals Under Uniaxial Loading, *Izv. Akad. Nauk SSSR*, *Mekh. Tverd. Tela*, 1972, no. 4, pp. 41–54.
17. Vildeman, V.E., Lomakin, E.V., and Tretyakov, M.P., Postcritical Deformation of Steels in Plane State, *Mech. Solids*, 2014, vol. 49, no. 1, pp. 18–26.
18. Vildeman, V.E. and Tretyakov, M.P., Material Testing by Plotting Total Deformation Curves, *J. Mach. Manuf. Reliab*., 2013, vol 42, no. 2, pp. 166–170.
19. Vildeman, V.E., Lomakin, E.V., Tretyakova, T.V., and Tretyakov, M.P., Development of Inhomogeneous Fields under Postcritical Deformation of Steel Specimens in Extension, *Mech. Solids*, 2016, vol. 51, no. 5, pp. 612–616.
20. Tretyakova, T.V. and Vildeman, V.E., *Space-Time Inhomogeneity of Inelastic Deformation in Metals*, Moscow: Fizmatlit, 2016.
21. Tretyakova, T.V. and Wildemann, V.E., Study of Spatial-Time Inhomogeneity of Serrated Plastic Flow Al-Mg Alloy: Using DIC-Technique, *Fract. Struct. Integr*., 2014, no. 27, pp. 83–97.
22. Lomakin, E.V., Tretyakova, T.V., and Vildeman, V.E., Effect of Quasi-Periodic Homogenization of Plastic Deformations in the Process of Tension of Samples of an Aluminum–Magnesium Alloy, *Dokl. Acad. Nauk*, 2015, vol. 60, no. 3, pp. 131–134.